



**HAL**  
open science

# First-principles DFT+ $U$ investigation of charged states of defects and fission gas atoms in CeO<sub>2</sub>

Lei Shi, Emerson Vathonne, Vincent Oison, Michel Freyss, Roland Hayn

► **To cite this version:**

Lei Shi, Emerson Vathonne, Vincent Oison, Michel Freyss, Roland Hayn. First-principles DFT+ $U$  investigation of charged states of defects and fission gas atoms in CeO<sub>2</sub>. *Physical Review B: Condensed Matter and Materials Physics (1998-2015)*, 2016, 94, pp.115132. 10.1103/PhysRevB.94.115132. cea-02063630

**HAL Id: cea-02063630**

**<https://cea.hal.science/cea-02063630>**

Submitted on 11 Mar 2019

**HAL** is a multi-disciplinary open access archive for the deposit and dissemination of scientific research documents, whether they are published or not. The documents may come from teaching and research institutions in France or abroad, or from public or private research centers.

L'archive ouverte pluridisciplinaire **HAL**, est destinée au dépôt et à la diffusion de documents scientifiques de niveau recherche, publiés ou non, émanant des établissements d'enseignement et de recherche français ou étrangers, des laboratoires publics ou privés.

**First-principles DFT+*U* investigation of charged states of defects and fission gas atoms in CeO<sub>2</sub>**Lei Shi,<sup>1,\*</sup> Emerson Vathonne,<sup>1</sup> Vincent Oison,<sup>2</sup> Michel Freyss,<sup>1</sup> and Roland Hayn<sup>2</sup><sup>1</sup>CEA, DEN, DEC, Centre de Cadarache, 13108 Saint-Paul-lez-Durance, France<sup>2</sup>Aix-Marseille Université, IM2NP, Campus Scientifique Saint-Jérôme, Case 142, 13397 Marseille Cedex 20, France

(Received 25 April 2016; revised manuscript received 27 July 2016; published 14 September 2016)

Cerium dioxide (CeO<sub>2</sub>) is considered as a model material for the experimental study of radiation damage in the standard nuclear fuel uranium dioxide (UO<sub>2</sub>). In this paper, we present a first-principles study in the framework of the DFT+*U* approach to investigate the charged point defects and the incorporation of the fission gases Xe and Kr in CeO<sub>2</sub> and compare it with published data in UO<sub>2</sub>. All intrinsic charge states are considered for point defects in contrast to previous published studies. Our calculations prove that CeO<sub>2</sub> shows similar behavior to UO<sub>2</sub> in the formation of point defects with the same charge states under stoichiometric and nonstoichiometric conditions. The charge states of vacancies have an important effect on the incorporation of fission gas atoms in CeO<sub>2</sub>. The bound Schottky defect with the two oxygen vacancies along the (100) direction is found to be energetically preferable to trap Xe and Kr atoms both in CeO<sub>2</sub> and UO<sub>2</sub>. Xe and Kr atoms in the cation vacancy sites under nonformal charge states (different from 4−) in CeO<sub>2</sub>, unlike in UO<sub>2</sub>, lose electrons to their neighboring atoms, which is traced back to the absence of the +5 valence state for Ce in contrast to its existence for U.

DOI: [10.1103/PhysRevB.94.115132](https://doi.org/10.1103/PhysRevB.94.115132)**I. INTRODUCTION**

The investigation of defects and impurities in oxide materials is a subject of high scientific interest, both for fundamental and applied sciences. First-principles studies are of great importance in that research field. For instance, taking native point defects in ZnO as a representative example, the influence of the proper charge state on the defect formation energies was demonstrated by Kohan *et al.* [1] In our following study, we concentrate on cerium dioxide (CeO<sub>2</sub>), an oxide of the rare-earth metal cerium, that has recently received great scientific interest due to its technical importance in a large number of applications. Generally, CeO<sub>2</sub> is widely used as automobile exhaust catalyst, electrolyte of solid oxide fuel cell (SOFC), oxygen storage device, etc. [2–6]. For experimental radiation damage studies in nuclear applications, CeO<sub>2</sub> could largely simulate UO<sub>2</sub>, having the same crystal structure, similar bulk properties and common features in the electronic structure with the advantage of being nonradioactive. That simplifies considerably any experimental study on radiation damage. Therefore a comparative study of the calculated defect and fission gas properties in UO<sub>2</sub> and CeO<sub>2</sub> is of particular interest as a first step to confirm the similarities of both oxides regarding radiation damage.

CeO<sub>2</sub> is an insulator with a 3 eV band gap [7,8]. The oxidation states of the atomic elements are, respectively, Ce<sup>4+</sup> and O<sup>2−</sup>. In CeO<sub>2</sub>, the 4*f* states remain completely unoccupied. However, the hybridization between Ce 4*f* orbitals and O 2*p* orbitals in the valence band has been demonstrated in the study of Wuilloud *et al.* [8]. In the case of nonstoichiometry, i.e., for oxygen deficient samples where Ce<sup>4+</sup> changes to the trivalent Ce<sup>3+</sup>, the chemical reduction of CeO<sub>2</sub> leads to the localization of one 4*f* electron on each Ce<sup>3+</sup> ion. Experimentally, in Ohno and Iwase's study [9,10], Ce<sup>3+</sup> ions are observed in the vicinity of oxygen vacancies created under irradiation with swift Xe ions by using extended

x-ray absorption fine structure (EXAFS) measurements, and a new peak of normalized intensity in x-ray photoelectron spectroscopy (XPS) spectrum is observed and corresponds to the Ce<sup>3+</sup> state in the valence band. Moreover, a ferromagnetic behavior is determined as an intrinsic property of reduced ceria due to the magnetic moments induced by the localized 4*f* electrons of the Ce<sup>3+</sup> ions [11]. This ferromagnetic behavior opens the way to possible spintronics applications of CeO<sub>2</sub>. The ratio of Ce<sup>3+</sup>/Ce<sup>4+</sup> is shown to be an important factor in the appearance of this magnetic property during irradiation experiments with neon ions [12,13].

To investigate CeO<sub>2</sub> including defects and impurities by a first-principles approach, the DFT+*U* method is used in this study in order to describe properly the localized 4*f* electrons in contrast to the standard DFT approach, which is clearly insufficient. Previous first-principles calculations have been performed to describe the ground-state properties of bulk cerium oxides (CeO<sub>2</sub> and Ce<sub>2</sub>O<sub>3</sub>) [14–20] and of CeO<sub>2</sub> with defects [21–37].

In order to get insight into the defect behavior in CeO<sub>2</sub> and to investigate an eventual similarity to UO<sub>2</sub>, we report here the results of a detailed first-principles study on defects and fission gases in CeO<sub>2</sub> and show that the proper charge state has an important influence, not only on the defect formation energy but also on the incorporation of fission gas atoms (Xe and Kr) in CeO<sub>2</sub>. The studies of Zacherle *et al.* [24] and Keating *et al.* [33] on point defects in CeO<sub>2</sub> already treated the influence of the charge states for the defects, but we will show that their results have to be completed by all possible intrinsic charge states. Xiao *et al.* [38] considered the trapping and diffusion of Xe in CeO<sub>2</sub> by taking into account only the neutral defects. In our study, we investigate the trapping behavior of Xe and another fission gas atom Kr in defect sites under various charge states. Furthermore, we improve the DFT+*U* calculations for charged defects in CeO<sub>2</sub> by a thorough use of the occupation matrix control (OMC) scheme. This scheme has to be used for a partially filled *f* shell as it was for instance demonstrated in the case of UO<sub>2</sub> [39,40] to avoid the metastable states, which were reported in several publications based on the

\*lei.shi@cea.fr

DFT+ $U$  approach [41–43]. In detail, we study the neutral and charged single-point defects by calculating their formation energies, and the fission gases Xe and Kr by calculating their incorporation energies in CeO<sub>2</sub>. We also investigate larger defects such as bound Schottky defects. Three regimes of stoichiometry are considered in the calculations: hypostoichiometric (oxygen-poor), stoichiometric, and hyperstoichiometric (oxygen-rich) conditions. By taking into account the necessary technical improvements in the theoretical description, we are able to obtain results that provide a new insight into the trapping properties of fission gases in CeO<sub>2</sub> and similar oxides.

## II. COMPUTATION DETAILS

The DFT calculations were all performed using the Vienna *ab initio* simulation package (VASP) code [44] in terms of the projector augmented wave method [45,46]. Both generalized gradient (GGA-PBE) [47] and local density approximations (LDA-CA) [48] have been considered to study the defect behavior. The valence electrons ( $5s^25p^64f^15d^16s^2$  for Ce and  $2s^22p^4$  for O) were treated using a plane wave basis set truncated by a cutoff energy of 500 eV. The core electrons are frozen and taken into account by using PAW atomic data. The same atomic data are used for the various oxidation states of each element. An additional on-site Coulomb repulsion was considered by including a Hubbard-like term proposed by Dudarev *et al.* in order to take into account the  $f$ -electron localization [49]. Based on the study of Castleton *et al.* [28], showing the  $U$ -parameter dependence of the Ce  $4f$  electron localization in the presence of the O vacancy, the optimum  $U$  value for Ce  $4f$  states in our study was selected to be 6.0 eV for LDA+ $U$  and 5.0 eV for GGA+ $U$  calculations. We did not take into account the Hubbard term for O  $2p$  states, which was considered in Keating *et al.*'s study in order to have a better description of localized holes on the O  $2p$  orbitals in presence of the Ce vacancy in CeO<sub>2</sub> [32,33]. However, in their study, the influence of the  $U$  parameter for O  $2p$  states was found negligible for the formation energies of point defects except the Ce vacancy [32]. It is to be noted that this influence for the Ce vacancy under its formal charge state (4<sup>-</sup>) is also negligible, because there is no localization of holes on the O  $2p$  orbitals, since the holes are electron compensated completely. In our study, we will show later that we find the charge state 4<sup>-</sup> to be the most favorable one for Ce vacancy in CeO<sub>2</sub>, justifying the fact that we can neglect the Hubbard term for O  $2p$  states.

The defect calculations were performed using a supercell containing 96 atoms, i.e., by doubling the conventional cell along the three lattice parameters, which is a standard supercell also used in the previous defect studies using DFT+ $U$  for CeO<sub>2</sub> [24,32,33,38] but also for UO<sub>2</sub> [50–52], with which we want to compare our results. Let us note that we verified the energy convergence with respect to the supercell size, by comparing the defect formation energies of neutral Ce and O vacancies obtained from calculations using supercells containing 96 and 324 atoms. We found a maximum difference of 0.14 eV on the defect formation energies between the two supercells. Thus we conclude that the calculations using a 96-atom supercell are a good compromise between accuracy and CPU time. In all calculations, the atomic positions and lattice parameters were optimized until forces acting in each

TABLE I. Bulk properties of CeO<sub>2</sub> calculated using LDA+ $U$  ( $U_{\text{eff}} = 6$  eV) and GGA+ $U$  ( $U_{\text{eff}} = 5$  eV) functionals and the comparison with experimental values.

Bulk properties	Experiments	LDA+ $U$	GGA+ $U$
Lattice constant (Å)	5.41 <sup>a</sup>	5.39	5.49
Bulk modulus (GPa)	220 <sup>a</sup> ,204 <sup>b</sup>	213	182
Band gap (eV)	3.0 <sup>c</sup>	2.7	2.5
$C_{11}$ (GPa)	403 <sup>b</sup>	386	344
$C_{12}$ (GPa)	105 <sup>b</sup>	127	101
$C_{44}$ (GPa)	60 <sup>b</sup>	71	54
$\Delta H_f^0$ (eV)	-11.30 <sup>d</sup>	-11.64	-10.52
$E_{\text{coh}}$ (eV)	-21.24 <sup>e</sup>	-18.30	-17.33

<sup>a</sup>Reference [53].

<sup>b</sup>Reference [54].

<sup>c</sup>References [7,8].

<sup>d</sup>Reference [55].

<sup>e</sup>Reference [56].

atom were less than 0.005 eV/Å and stress components were less than 0.01 kbar.

We first conduct bulk property calculations on the perfect CeO<sub>2</sub> crystal in order to have a comparative investigation on the difference of calculated results between the LDA+ $U$  and GGA+ $U$  functional. Table I presents the experimental and calculated values of some bulk properties of CeO<sub>2</sub>: lattice constant, bulk modulus, band gap, elastic constants, enthalpy of formation and cohesive energy. The bulk properties calculated using both LDA+ $U$  and GGA+ $U$  are in good agreement with the experimental values. However, we see that LDA+ $U$  reproduces slightly better electronic properties such as the band gap as well as some other bulk properties of CeO<sub>2</sub> (lattice constant, bulk modulus, cohesive energy and enthalpy of formation) than GGA+ $U$ . Therefore, for all the following calculations considering the defect formation energies and fission gas incorporation energies, we will mainly use the LDA+ $U$  functional.

In the study of defects, in order to avoid the metastable states yielded by the DFT+ $U$  method, the occupation matrix control (OMC) scheme was used following the scheme implemented by Jomard *et al.* [41] and Amadon *et al.* [42]. The OMC scheme distinguishes the ground state from metastable states based on the total energy of the system, as detailed in the study of UO<sub>2</sub> by Dorado *et al.* [39]. For CeO<sub>2</sub>, the electronic ground state of the supercell containing a neutral oxygen vacancy involves the localization of electrons, initially localized on the removed oxygen atom, on two of four adjacent cerium atoms, leading to the formation of two Ce<sup>3+</sup> ions. A DFT+ $U$  calculation of CeO<sub>2</sub> with oxygen defects without an adequate preconditioning method yields the distribution of charges on several adjacent Ce ions and fails to reach the system ground state with localized  $4f$  electrons on Ce<sup>3+</sup> ions. To solve this problem by using the OMC scheme, the proper  $4f$  electron occupation matrix that corresponds to the Ce<sup>3+</sup> ions on which the  $4f$  electrons are localized should be determined in the first place.

In order to find this occupation matrix corresponding to the Ce<sup>3+</sup> ions, we used an approach proposed by Zacherle *et al.* [24] in the calculation of an electron polaron. The

additional electron is well localized on the chosen Ce ion if we displace all the neighboring atoms (both Ce and O atoms) as a preconditioning before the structure relaxation. With this approach, we succeed to obtain the occupation matrix corresponding to the  $\text{Ce}^{3+}$  ion with one  $4f$  electron localized. By applying this matrix in the calculation of the  $\text{CeO}_2$  supercell containing one neutral oxygen vacancy, we find that the  $4f$  electrons are well localized on two of the four first neighboring Ce ions in the vicinity of the oxygen vacancy. And the corresponding system energy is about  $13 \text{ meV}/(\text{CeO}_2)$  lower than the one when the electrons are distributed on the adjacent Ce ions without forming  $\text{Ce}^{3+}$ . In addition, by using the OMC scheme, we could even control the positions of the  $\text{Ce}^{3+}$  ions on which the electrons are localized. Our study shows that the localization of  $4f$  electrons on either two of the four first neighboring Ce ions results in the ground state of  $\text{CeO}_2$  with one neutral oxygen vacancy.

### III. DEFECT FORMATION AND FISSION GAS INCORPORATION

#### A. Formation energies of charged defects

We first investigate the formation of charged single defects in  $\text{CeO}_2$ . The defect formation energy for a defect  $X$  in the charge state  $q$ ,  $E_{\text{form}}(X^q)$ , is obtained using the standard expression:

$$E_{\text{form}}(X^q) = E_{\text{tot}}(X^q) - \left( E_{\text{tot}}(\text{bulk}) - \sum_i n_i \mu_i \right) + q(E_{\text{Fermi}} + E_{\text{VBM}}) + E_{\text{corr}}, \quad (1)$$

where  $E_{\text{tot}}(X^q)$  is the total energy of the supercell containing the charged defect, and  $E_{\text{tot}}(\text{bulk})$  is the total energy of the perfect bulk supercell.  $n_i$  is the number of atoms of type  $i$  removed from ( $n_i > 0$ ) or added to ( $n_i < 0$ ) the bulk cell to form the vacancy and interstitial defects, respectively, and  $\mu_i$  is the corresponding chemical potential.  $E_{\text{Fermi}}$  is the Fermi energy in the range of the band gap, which corresponds to the electron chemical potential. The zero energy of  $E_{\text{Fermi}}$  is fixed at the valence-band maximum ( $E_{\text{VBM}}$ ) of the perfect supercell. An energy correction term,  $E_{\text{corr}}$ , is proposed by Taylor and Bruneval for the calculation of charged defect formation energies in a finite-size supercell as follows [57]:

$$E_{\text{corr}} = \Delta E_{\text{el}} + q \Delta V. \quad (2)$$

$\Delta E_{\text{el}}$  is the Madelung term [58,59], which corrects the spurious long-ranged electrostatic interaction between the charged defect and its periodic images.  $\Delta V$  is a potential alignment term, which corrects the shifted band structure of defective supercells relative to the perfect supercell. For the moment, the computational resources available do not allow to take into account a sufficiently large supercell in order to neglect these two corrections.  $\Delta E_{\text{el}}$  and  $\Delta V$  are expressed as

$$\Delta E_{\text{el}} = \frac{\alpha q^2}{2\epsilon_0 L} \quad (3)$$

and

$$\Delta V = \langle v_{\text{KS}}^{\text{bulk}} \rangle - \langle v_{\text{KS}}^{\text{defect}} \rangle, \quad (4)$$

where  $\epsilon_0$  is the static dielectric constant chosen as the experimental value 23 for  $\text{CeO}_2$  [60].  $L$  is the length of the supercell edge.  $\alpha$  is the Madelung lattice constant, which is 2.519 for a fluorite structure [61].  $\langle v_{\text{KS}}^{\text{bulk}} \rangle$  is the average Kohn-Sham potential in the perfect supercell and  $\langle v_{\text{KS}}^{\text{defect}} \rangle$  is the average Kohn-Sham potential in the supercell with defects. These potentials are the results of the DFT+*U* calculations.

In Eq. (1), the chemical potentials  $\mu_i$  correspond to the cerium and oxygen chemical potentials  $\mu_{\text{Ce}}^{\text{CeO}_2}$  and  $\mu_{\text{O}}^{\text{CeO}_2}$  in  $\text{CeO}_2$ . They cannot be obtained directly from the DFT+*U* calculations because they depend, in particular, on the stoichiometry and the partial pressure of oxygen [ $P(\text{O}_2)$ ]. To calculate the values of  $\mu_{\text{Ce}}^{\text{CeO}_2}$  and  $\mu_{\text{O}}^{\text{CeO}_2}$ , accessible under different stoichiometry conditions, we use a method based on the study of Na-Phattalung *et al.* [62] and Hong *et al.* [63] considering the standard enthalpy of formation for various phases of the Ce-O system. For  $\text{CeO}_2$ , the standard enthalpy of formation is defined as

$$\Delta H_f^0(\text{CeO}_2) = \mu_{\text{CeO}_2}^{\text{bulk}} - \mu_{\text{Ce}}^{\text{Ce met.}} - 2\mu_{\text{O}}^{\text{O}_2}, \quad (5)$$

where  $\mu_{\text{Ce}}^{\text{Ce met.}}$  is the Ce chemical potential in its standard metallic  $\alpha$ -cerium state and  $\mu_{\text{O}}^{\text{O}_2}$  is the O chemical potential in its standard oxygen gas state. For bulk  $\text{CeO}_2$ , the chemical potential is a constant value given by

$$\mu_{\text{CeO}_2}^{\text{bulk}} = \mu_{\text{Ce}}^{\text{CeO}_2} + 2\mu_{\text{O}}^{\text{CeO}_2}. \quad (6)$$

We introduce two variables  $\Delta\mu_{\text{Ce}}$  and  $\Delta\mu_{\text{O}}$  of the chemical species with respect to their standard states, defined as

$$\Delta\mu_{\text{Ce}} = \mu_{\text{Ce}}^{\text{CeO}_2} - \mu_{\text{Ce}}^{\text{Ce met.}}, \quad (7)$$

$$\Delta\mu_{\text{O}} = \mu_{\text{O}}^{\text{CeO}_2} - \mu_{\text{O}}^{\text{O}_2}, \quad (8)$$

Let us note that the values  $\Delta\mu_{\text{Ce}}$  and  $\Delta\mu_{\text{O}}$  should be negative otherwise the  $\text{CeO}_2$  crystal would decompose. The enthalpy of formation of  $\text{CeO}_2$  can then be expressed as

$$\Delta H_f^0(\text{CeO}_2) = \Delta\mu_{\text{Ce}} + 2\Delta\mu_{\text{O}}. \quad (9)$$

This gives an accessible range of the values of both chemical potential variables  $\Delta\mu_{\text{Ce}}$  and  $\Delta\mu_{\text{O}}$ :

$$\Delta H_f^0(\text{CeO}_2) < \Delta\mu_{\text{Ce}} < 0$$

and

$$\frac{1}{2}\Delta H_f^0(\text{CeO}_2) < \Delta\mu_{\text{O}} < 0.$$

In our LDA+*U* calculations, the value of  $\Delta H_f^0(\text{CeO}_2)$  is  $-11.64 \text{ eV}$ , as reported in Table I. Thus the accessible ranges of  $\Delta\mu_{\text{Ce}}$  and  $\Delta\mu_{\text{O}}$  are determined as

$$-11.64 \text{ eV} < \Delta\mu_{\text{Ce}} < 0 \text{ eV}$$

and

$$-5.82 \text{ eV} < \Delta\mu_{\text{O}} < 0 \text{ eV}.$$

In order to further narrow the ranges of  $\Delta\mu_{\text{Ce}}$  and  $\Delta\mu_{\text{O}}$ , we consider the other oxide phase of the Ce-O system,  $\text{Ce}_2\text{O}_3$ , and put a constraint on  $\Delta\mu_{\text{Ce}}$  and  $\Delta\mu_{\text{O}}$  to take into account the relative stability of  $\text{CeO}_2$  compared to  $\text{Ce}_2\text{O}_3$ . In analogy

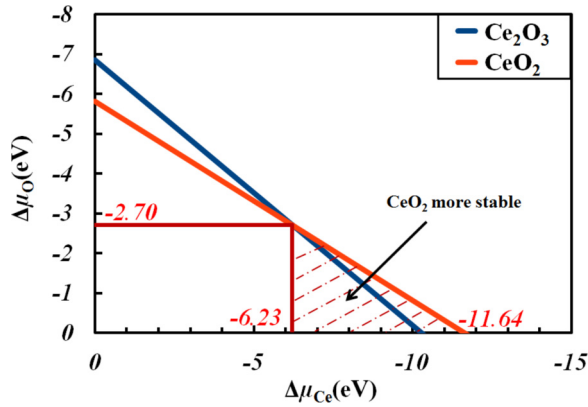


FIG. 1.  $\Delta\mu_{\text{Ce}}$  as a function of  $\Delta\mu_{\text{O}}$  for different phases of the Ce-O systems:  $\text{CeO}_2$  in red and  $\text{Ce}_2\text{O}_3$  in dark blue.

to Eq. (9), the standard enthalpy of formation of  $\text{Ce}_2\text{O}_3$  is expressed as follows:

$$\Delta H_f^0(\text{Ce}_2\text{O}_3) = 2\Delta\mu_{\text{Ce}} + 3\Delta\mu_{\text{O}}. \quad (10)$$

The calculated value of  $\Delta H_f^0(\text{Ce}_2\text{O}_3)$  is  $-20.57$  eV using LDA+ $U$ , which is close to the experimental value of  $-18.60$  eV [55]. In Fig. 1, we determine the relative stability of each phase by plotting  $\Delta\mu_{\text{Ce}}$  as a function of  $\Delta\mu_{\text{O}}$  for  $\text{CeO}_2$  and  $\text{Ce}_2\text{O}_3$ , respectively. And we can see that  $\text{CeO}_2$  is more stable than  $\text{Ce}_2\text{O}_3$  when  $\Delta\mu_{\text{Ce}}$  is lower than  $-6.23$  eV and  $\Delta\mu_{\text{O}}$  is larger than  $-2.70$  eV. This stability of  $\text{CeO}_2$  compared with  $\text{Ce}_2\text{O}_3$  determines a range accessible for  $\Delta\mu_{\text{Ce}}$  and  $\Delta\mu_{\text{O}}$  as follows:

$$-11.64 \text{ eV} < \Delta\mu_{\text{Ce}} < -6.23 \text{ eV}$$

and

$$-2.70 \text{ eV} < \Delta\mu_{\text{O}} < 0 \text{ eV}.$$

The calculated values of  $\mu_{\text{Ce}}^{\text{met.}}$  and  $\mu_{\text{O}}^{\text{O}_2}$  are  $-4.55$  and  $-5.24$  eV, respectively, by our LDA+ $U$  calculations. Note that in our study, we did not apply any correction for the DFT calculated binding energy of the  $\text{O}_2$  molecule [64], which come into play in the term  $\mu_{\text{O}}^{\text{O}_2}$ . The well-known misestimation of the  $\text{O}_2$  binding energy can be corrected, as suggested by Lee *et al.* [65], Wang *et al.* [66] and Grindy *et al.* [67], by fitting a correction to the calculated formation enthalpy of several metal oxides. However, Grindy *et al.* showed that the energy correction is small using the LDA functional (0.25 eV/ $\text{O}_2$ ) [67]. And it was further emphasized by Lee *et al.* that applying the DFT+ $U$  method reduces even more the error from pure DFT in the calculation of formation enthalpies of oxides [65].

After applying our values of  $\mu_{\text{Ce}}^{\text{met.}}$  and  $\mu_{\text{O}}^{\text{O}_2}$  into Eqs. (7) and (8), we could finally determine the accessible ranges for the chemical potentials  $\mu_{\text{Ce}}^{\text{CeO}_2}$  and  $\mu_{\text{O}}^{\text{CeO}_2}$  in  $\text{CeO}_2$ :

$$-16.19 \text{ eV} < \mu_{\text{Ce}}^{\text{CeO}_2} < -10.78 \text{ eV}$$

and

$$-5.24 \text{ eV} > \mu_{\text{O}}^{\text{CeO}_2} > -7.94 \text{ eV}.$$

In this study, we have considered three limiting cases, depending on the stoichiometry: (1) the oxygen-rich conditions,

TABLE II. The accessible values of chemical potentials  $\mu_{\text{Ce}}^{\text{CeO}_2}$  and  $\mu_{\text{O}}^{\text{CeO}_2}$  in  $\text{CeO}_2$  calculated by LDA+ $U$  and GGA+ $U$  functionals under various stoichiometry conditions.

Functional	Stoichiometry	$\mu_{\text{Ce}}^{\text{CeO}_2}$ (eV)	$\mu_{\text{O}}^{\text{CeO}_2}$ (eV)
LDA+ $U$	O-poor	-10.78	-7.94
	O-rich	-16.19	-5.24
	Stoichiometric	-13.48	-6.59
GGA+ $U$	O-poor	-10.09	-7.17
	O-rich	-14.58	-4.93
	Stoichiometric	-12.34	-6.05

where  $\mu_{\text{O}}^{\text{CeO}_2}$  is maximum and  $\mu_{\text{Ce}}^{\text{CeO}_2}$  is minimum; (2) the oxygen-poor conditions, where  $\mu_{\text{O}}^{\text{CeO}_2}$  is minimum and  $\mu_{\text{Ce}}^{\text{CeO}_2}$  is maximum; and (3) the stoichiometric conditions, where both  $\mu_{\text{O}}^{\text{CeO}_2}$  and  $\mu_{\text{Ce}}^{\text{CeO}_2}$  take their mean values.

The corresponding values of  $\mu_{\text{Ce}}^{\text{CeO}_2}$  and  $\mu_{\text{O}}^{\text{CeO}_2}$  calculated by both LDA+ $U$  and GGA+ $U$  functionals under these three stoichiometry conditions are reported in Table II. The GGA+ $U$  results obtained with the calculated enthalpies of formation,  $\Delta H_f^0(\text{CeO}_2) = -10.52$  eV and  $\Delta H_f^0(\text{Ce}_2\text{O}_3) = -18.8$  eV using GGA+ $U$ , are very identical to those obtained by Zacherle *et al.* [24].

## B. Incorporation of fission products in charged defects

In order to investigate the trapping properties of gaseous fission products ( $FP$ ) in  $\text{CeO}_2$ , we determine their incorporation energies in charged defect sites. The incorporation energies are given using the following general expression:

$$E_{\text{inc}}(FP, X) = E_{\text{tot}}(FP, X) - E_{\text{tot}}(X) - E_{\text{tot}}(FP), \quad (11)$$

where  $E_{\text{tot}}(FP, X)$  is the total energy of the supercell containing a fission product incorporated in the defect site  $X$ ;  $E_{\text{tot}}(X)$  is the total energy of the supercell containing the defect site  $X$ ; and  $E_{\text{tot}}(FP)$  is the total energy of the isolated fission product. In order to consider the various charge states of the defect site in  $\text{CeO}_2$ , the incorporation energy is expressed as a function of the formation energy of the defect site and the solution energy of the fission product in the defect site. This gives

$$E_{\text{inc}}(FP, X) = E_{\text{sol}}(FP, X^{q'}) - E_{\text{form}}(X^{q'}), \quad (12)$$

where  $E_{\text{sol}}(FP, X^{q'})$  is the solution energy of the fission product in defect site  $X$  with the most stable charge state  $q'$ :

$$E_{\text{sol}}(FP, X^{q'}) = E_{\text{tot}}(FP, X^{q'}) - \left( E_{\text{tot}}(\text{bulk}) - \sum_j n_j \mu_j \right) + q'(E_{\text{Fermi}} + E_{\text{VBM}}) + \Delta E'_{\text{el}} + q' \Delta V'. \quad (13)$$

Herein  $E_{\text{tot}}(FP, X^{q'})$  is the total energy of the supercell containing the fission product incorporated in the defect site  $X$  under charge state  $q'$ .  $\mu_j$  is the chemical potential of the species  $j$  (fission product atoms, Ce and O atoms) added or removed with respect to the perfect supercell of  $\text{CeO}_2$ .  $\Delta E'_{\text{el}}$  is

the Madelung term and  $\Delta V'$  is the potential alignment term as defined in Eqs. (3) and (4), respectively. The term  $E_{\text{form}}(X^q)$  is the formation energy of the defect site  $X$  in its charge state  $q$  obtained from Eq. (1). Thus the incorporation energy of the fission product in the charged defect site is expressed as a function of the Fermi energy as

$$E_{\text{inc}}(FP, X) = E_{\text{tot}}(FP, X^{q'}) - E_{\text{tot}}(X^q) - n_{FP}\mu_{FP} + (q' - q)(E_{\text{Fermi}} + E_{\text{VBM}}) + (\Delta E'_{\text{el}} - \Delta E_{\text{el}}) + (q'\Delta V' - q\Delta V). \quad (14)$$

In this equation,  $\mu_{FP}$  is the chemical potential of the fission product in the standard isolated state. Let us note that the chemical potentials  $\mu_{\text{Ce}}^{\text{CeO}_2}$  and  $\mu_{\text{O}}^{\text{CeO}_2}$  do not appear explicitly. Therefore  $E_{\text{inc}}(FP, X)$  does not depend on the stoichiometry conditions.

We introduce a term  $\Delta q = q' - q$ . When  $\Delta q = 0$ , which means that the most stable charge state of the defect site  $X$  does not change after trapping the fission product, the incorporation energy becomes independent of the Fermi energy  $E_{\text{Fermi}}$  and can be expressed as

$$E_{\text{inc}}(FP, X) = E_{\text{tot}}(FP, X^q) - E_{\text{tot}}(X^q) - n_{FP}\mu_{FP} + q(\Delta V' - \Delta V). \quad (15)$$

In this study, two gaseous fission products are considered, Xe and Kr. The corresponding results are presented in Sec. V.

#### IV. RESULTS ON THE DEFECT FORMATION

##### A. Density of states of CeO<sub>2</sub> containing the neutral oxygen vacancy

In order to have an insight into the influence of defects on the electron structure of CeO<sub>2</sub>, we firstly compare the calculated total density of states of perfect CeO<sub>2</sub> with the one including a neutral O vacancy by LDA+*U* in Fig. 2. The valence band mainly consists of O 2*p* states, whereas the conduction band mainly consists of Ce 4*f* states. In bulk CeO<sub>2</sub>, the band gap is

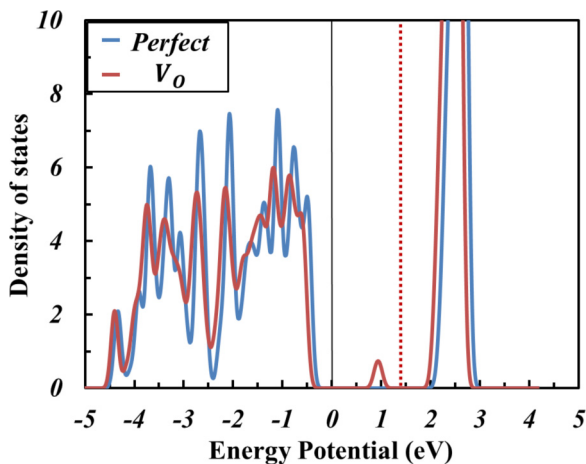


FIG. 2. Total density of states of perfect CeO<sub>2</sub> and the one including a neutral O vacancy ( $V_{\text{O}}$ ). The Fermi level of the perfect cell is fixed at 0 eV. The dashed red line is the corresponding Fermi level for  $V_{\text{O}}$ .

found to be 2.7 eV, in good agreement with the experimental value of 3 eV.

When a neutral O vacancy is created, the two extra electrons of the removed O atom are localized on two of the four adjacent Ce atoms. This forms two  $\text{Ce}^{3+}$  ions, which present a ferromagnetic order, and affects the density of states. An additional electronic state appears in the band gap 1.3 eV above the maximum of the valence band. Consequently, the Fermi level is shifted by 1.4 eV towards the conduction band, indicating that O neutral vacancies involve  $n$  doping of CeO<sub>2</sub>.

However, we should note that when considering a charged O vacancy as well as a charged Ce vacancy under their formal charge states +2 and -4, respectively, the electronic doping is canceled due to the compensation of charges. Thus the resulting density of states remains nearly the same as the one of bulk CeO<sub>2</sub>.

##### B. Formation energies of charged point defects in CeO<sub>2</sub>

We present here the results on the formation energies of defects under various charge states, considering three types of stoichiometry conditions. The formation energies are calculated as a function of the Fermi energy in the range of the band gap according to Eq. (1).

###### 1. Small point defects

We first study the small point defects: the monovacancies ( $V_{\text{O}}$  and  $V_{\text{Ce}}$ ), the monointerstitials ( $I_{\text{O}}$  and  $I_{\text{Ce}}$ ) and divacancy ( $V_{\text{O}}+V_{\text{Ce}}$ ). Figure 3 presents the comparison between the LDA+*U* and GGA+*U* results under the stoichiometric conditions. For each defect, the most stable charge state depends on the Fermi energy value in the band gap and is given above the curves. Overall good agreement is found between these two functionals in the calculated formation energies of each defect. The oxygen vacancy has the lowest formation energy and is the most stable defect. We can see that the charge states shown on the curves of each defect are quite similar between LDA+*U* and GGA+*U*, and the most stable charge states of each defect for the Fermi level in the middle of the band gap are consistent to the ionic picture:  $V_{\text{O}}^{2+}$ ,  $V_{\text{Ce}}^{4-}$ ,  $I_{\text{O}}^{2-}$ , and  $I_{\text{Ce}}^{4+}$ . They are the formal charge states of the corresponding defects.

In the vicinity of a neutral oxygen vacancy, by using the occupation matrix control (OMC) scheme, we managed to localize the 4*f* electrons on the *f* orbitals of two adjacent Ce ions to form  $\text{Ce}^{3+}$  ions in both LDA+*U* and GGA+*U* functional calculations. And in the case of a neutral cerium vacancy, the extra positive charge of the removed Ce atom is distributed on the neighboring O atoms and creates holes on the 2*p* orbitals. As shown by Keating *et al.*, the hole localization is expected when the *U* parameter for O 2*p* states is considered [32,33]. However, there is no such hole localization in the presence of a Ce vacancy under its formal charge state (4-), because the holes are fully compensated by electrons. And as seen in both Figs. 3 and 4, (4-) is the most stable charge state of Ce vacancies for the Fermi level in a wide range of the band gap from 0.6 to 3.0 eV by both LDA+*U* and GGA+*U* calculations. The hole localization on O 2*p* states in the presence of Ce vacancies under nonformal charge states (different from 4-) would thus occur for Fermi energies close to the valence-band maximum, where the formation energies

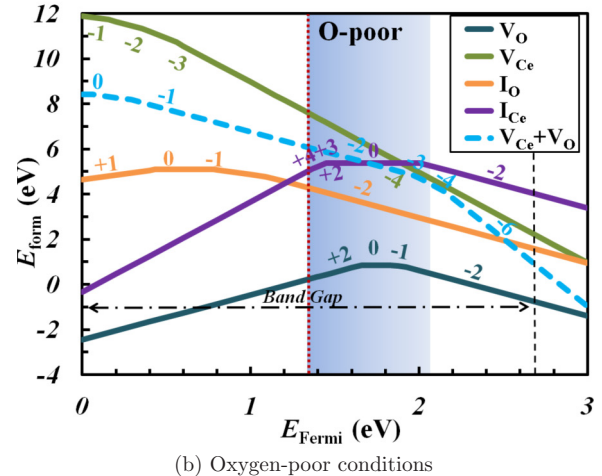
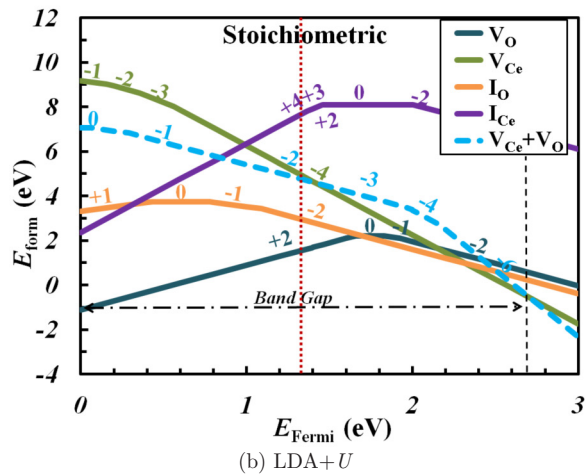
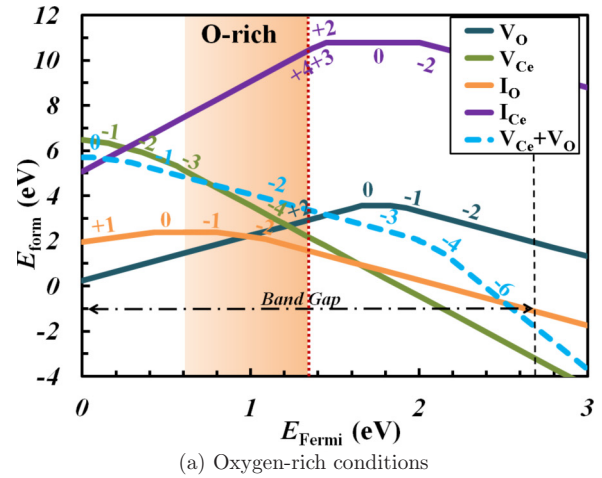
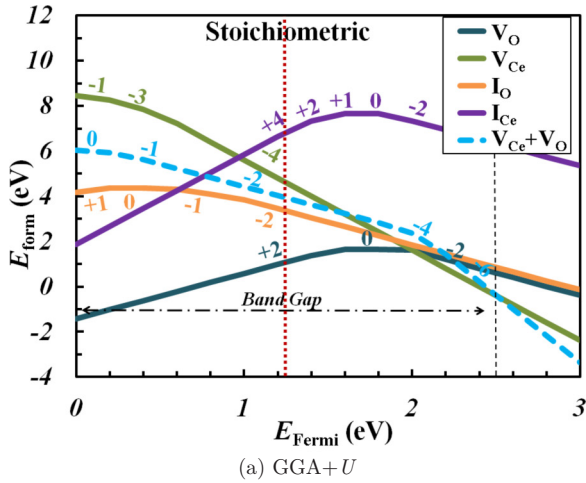


FIG. 3. Formation energy of charged point defects (O vacancy  $V_O$ , O interstitial  $I_O$ , Ce vacancy  $V_{Ce}$ , Ce interstitial  $I_{Ce}$ , and divacancy) calculated using GGA+ $U$  and LDA+ $U$  as a function of the Fermi energy for  $CeO_2$  under stoichiometric conditions.

FIG. 4. Formation energy of charged point defects (O vacancy  $V_O$ , O interstitial  $I_O$ , Ce vacancy  $V_{Ce}$ , Ce interstitial  $I_{Ce}$ , and divacancy) calculated using LDA+ $U$  as a function of the Fermi energy for  $CeO_2$  under O-rich and O-poor conditions, respectively.

of Ce vacancies are very large anyway. Therefore we suppose that the influence of this hole localization on O  $2p$  orbitals is not significant in our discussion of the relative stability of point defects in  $CeO_2$  and the comparison with  $UO_2$ .

Figure 4 presents the results under oxygen-rich and oxygen-poor conditions using the LDA+ $U$  functional. The regions in color blue and orange shown in Fig. 4 (and Fig. 6) present the ranges of energy towards which the Fermi level is shifted in oxygen-poor and oxygen-rich conditions. In both stoichiometry conditions, the most stable charge states of the corresponding defects are consistent to the ionic picture ( $V_O^{2+}$ ,  $V_{Ce}^{4-}$ ,  $I_O^{2-}$ , and  $I_{Ce}^{4+}$ ). The  $V_O$  is the most stable defect under O-poor conditions. Comparing our results with the ones by Zacherle *et al.* [24] and Keating *et al.* [33], we found that the point defect formation energies are similar only in the region where the charge states considered are identical. In our study, we considered additional intrinsic charges for the point defects and could thus find differences in the stability of point defects compared to the previous studies. In particular, for  $V_O$  with the Fermi level close to the conduction-band minimum,  $V_O^{2-}$  becomes more stable than the neutral  $V_O$  under all stoichiometry conditions.

For the O interstitial, it is to be noted that we only considered the  $I_O$  in the octahedral site rather than the peroxide O interstitial (O dumbbell) in  $CeO_2$ . That is because our study focuses on the similarities of defect properties between  $CeO_2$  and  $UO_2$ , and the O dumbbell in  $UO_2$  is less stable than a single O interstitial according to the study of Middleburgh *et al.* [68].

## 2. Bound Schottky defects

The bound Schottky defects (BSD) are considered to investigate the formation of larger point defects. The BSD consists of one  $CeO_2$  vacancy in the supercell (one Ce and two O adjacent vacancies). There are basically three BSD configurations, which depend on the positions of oxygen vacancies in the Ce-centered oxygen cage as shown in Fig. 5.

The formation energies of the bound Schottky defects are presented in Fig. 6 under stoichiometric conditions since they are stoichiometric defects. They do not depend on the values of the O and Ce chemical potentials. We can see that the formation energies of all three bound Schottky defects are in the range between 5.0 to 5.5 eV for the Fermi level near the middle of the band gap. The BSDs with oxygen vacancies along the (110) and (111) directions (BSD2 and BSD3) give the lowest

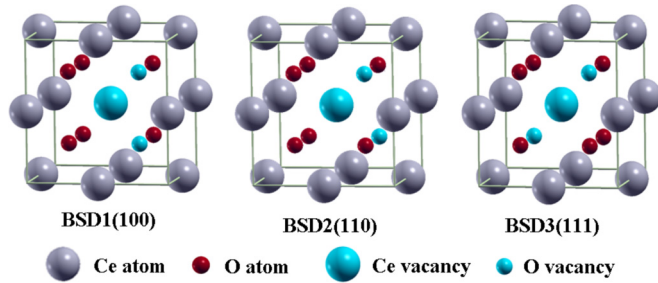


FIG. 5. Three configurations of bound Schottky defects based on the  $V_O$ - $V_{Ce}$ - $V_O$  angle: BSD1 with O vacancies along the (100) direction; BSD2 with O vacancies along the (110) direction; and BSD3 with O vacancies along the (111) direction.

formation energies for a wide range of Fermi energy near the middle of the band gap. These are the two configurations of BSDs with the two oxygen vacancies that are farther away from each other. The ionic character of  $CeO_2$  is also confirmed. The neutral charge state is favored for the most stable BSDs (BSD2 and BSD3) for the Fermi level up to around 2 eV, which is again consistent with the ionic character of  $CeO_2$ . Between 1.5 and 2.0 eV also the nonnormal charge state ( $-1$ ) of BSD1 becomes as stable as the neutral states of BSD2 and BSD3. And the formation energies of all the three BSDs are becoming similar with each other with a charge state  $-2$  for a Fermi level position in the vicinity of the conduction-band minimum.

### 3. Comparison with $UO_2$

The results obtained for the defect formation using LDA+*U* for  $CeO_2$  are compared here with the ones obtained in  $UO_2$  using GGA+*U* in Vathonne *et al.*'s study [50]. This comparison between the results obtained using the two different LDA+*U* and GGA+*U* approximations is made possible by the overall good agreement between the LDA+*U* and GGA+*U* results on point defect formation in  $CeO_2$  (shown in Fig. 3). Viewing the defect formation energy graphs for  $CeO_2$  and  $UO_2$  (Ref. [50, Fig. 3]) under stoichiometric and nonstoichiometric conditions, we observe great similarities in the formation energy of each defect between those two compounds. The relative stability of the defects as a function of the Fermi energy follows the same trends for  $CeO_2$  and  $UO_2$ . Moreover,

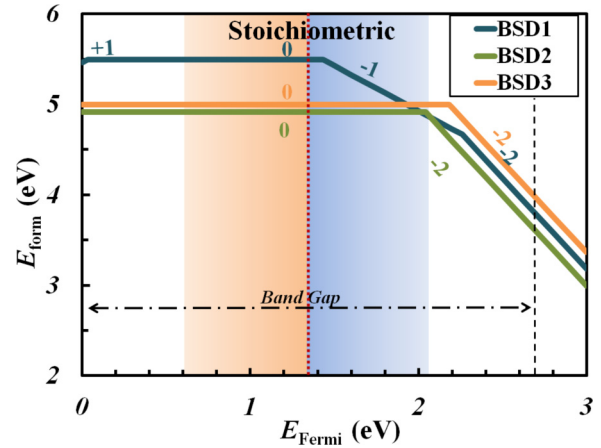


FIG. 6. Formation energy of charged bound Schottky defects (BSD) calculated using LDA+*U* as a function of the Fermi energy for  $CeO_2$ .

the most stable charge states of each defect in  $CeO_2$  are all in good agreement with the ones in  $UO_2$ .

Table III presents the calculated formation energies of defects in both  $CeO_2$  and  $UO_2$  under three different stoichiometry conditions and for the Fermi energy in the middle of the band gap. We can see that the most stable charge state of each defect for the Fermi level in the middle of the band gap is consistent to the ionic character of both compounds (except the uranium interstitial in  $UO_2$ ), which means that there are no additional electrons localized or holes formed on the cation *f* orbitals or oxygen *p* orbitals, respectively. The formation energy values of oxygen vacancies and cation interstitials ( $V_O$  and  $I_{Ce}$ ) in  $CeO_2$  are quite similar to the ones in  $UO_2$  with differences between 0.2 and 0.5 eV. However, when considering other types of defects ( $I_O$ ,  $V_{Ce|U}$ , and divacancy), the differences rise to a range between 1.6 and 2.8 eV. That can be explained by the fact that it is more easy to stabilize O-rich compounds in  $UO_2$  than in  $CeO_2$ . For instance, there exist stable compounds  $U_4O_9$ ,  $U_3O_8$  and  $UO_3$  besides  $UO_2$ . However, this is not the case for Ce-O compounds, where only  $CeO_2$  and  $Ce_2O_3$  are stable oxides [69]. In other words, U can have the valency up to  $U^{6+}$  in  $UO_3$ , which is not the case for Ce. This is the fundamental difference between  $CeO_2$  and  $UO_2$ , which leads

TABLE III. Formation energies (eV) and the most stable charge states of various defects for the Fermi energy in the middle the band gap in  $CeO_2$  using LDA+*U* under various stoichiometry conditions and the comparison with  $UO_2$  using GGA+*U*.

Defects	O-rich		Stoichiometric		O-poor		Charge state	
	$CeO_2$	$UO_2^a$	$CeO_2$	$UO_2^a$	$CeO_2$	$UO_2^a$	$CeO_2$	$UO_2^a$
$V_O$	2.90	2.58	1.56	1.29	0.21	0.00	+2	+2
$V_{Ce U}$	2.23	0.00	4.94	2.58	7.64	5.16	-4	-4
$V_{Ce U}+V_O$	3.40	0.68	4.75	1.97	6.11	3.26	-2	-2
$I_O$	1.60	0.06	2.95	1.35	4.30	2.64	-2	-2
$I_{Ce U}$	10.39	10.70	7.68	8.12	4.98	5.54	+4	+3
BSD1	-	-	5.49	3.25	-	-	0	0
BSD2	-	-	4.91	2.47	-	-	0	0
BSD3	-	-	5.00	2.60	-	-	0	0

<sup>a</sup>Reference [50].

to higher formation energies of oxygen interstitials and cation vacancies (but also divacancy) in  $\text{CeO}_2$  than in  $\text{UO}_2$ .

For bound Schottky defects, the BSD2 and BSD3 are the most stable configurations (with the BSD2 having a slightly lower formation energy than the BSD3) in both  $\text{UO}_2$  and  $\text{CeO}_2$  for the Fermi energy near the middle of the band gap. The formation energies of all the BSDs in  $\text{CeO}_2$  are about 2.2–2.4 eV higher than the ones in  $\text{UO}_2$ , which can be linked to the higher formation energies of cation vacancies in  $\text{CeO}_2$  compared to  $\text{UO}_2$ .

Now we compare the point defects under neutral and nonnormal charge states between  $\text{CeO}_2$  and  $\text{UO}_2$ . In the presence of  $\text{V}_\text{O}$  and  $\text{I}_{\text{Ce|U}}$ , the extra available electrons are localized on the f orbitals of adjacent cations to form  $\text{Ce}^{3+}$  and  $\text{U}^{3+}$ . In the presence of other neutral defects such as  $\text{V}_{\text{Ce|U}}$ ,  $\text{I}_\text{O}$ , and divacancy, there are no  $\text{Ce}^{5+}$  ions in  $\text{CeO}_2$  unlike in  $\text{UO}_2$  in which  $\text{U}^{5+}$  ions can be formed. The formation of  $\text{Ce}^{5+}$  would require the removal of one electron from the fully occupied bands of  $\text{Ce}^{4+}$  ions, which is very unfavorable. Indeed, the fifth ionization energy of Ce is high (it is estimated as 65.55 eV in the study of Reader and Epstein [70]) compared to fifth ionization energy of U (45.77 eV based on Pyper *et al.*'s study [71]) and also in comparison to the electron affinity of  $\text{Ce}^{4+}$  to form  $\text{Ce}^{3+}$ , which is 36.76 eV [72].

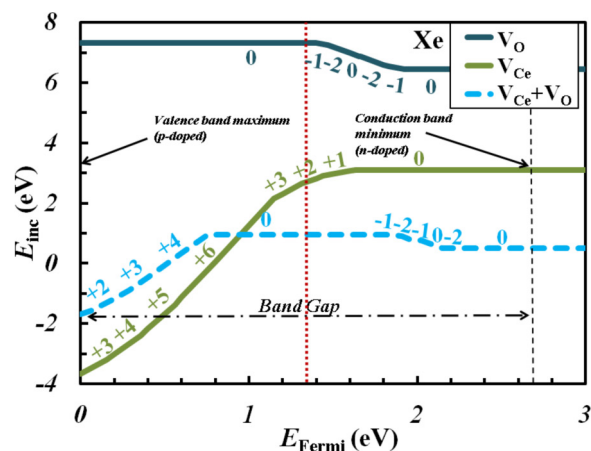
We should note that our study of defects in  $\text{CeO}_2$  and the comparison to  $\text{UO}_2$  do not take into account the effect of the temperature. Temperature may have an influence on the defect formation energies due, in particular, to the temperature dependence of the oxygen molecule chemical potential, as studied by Mastrikov *et al.* [73]. However, our objective is to focus on the physics of point defects in  $\text{CeO}_2$  and the comparison to  $\text{UO}_2$ , regardless of the conditions of use of these materials.

## V. INVESTIGATION OF XE AND KR TRAPPING PROPERTIES IN $\text{CeO}_2$

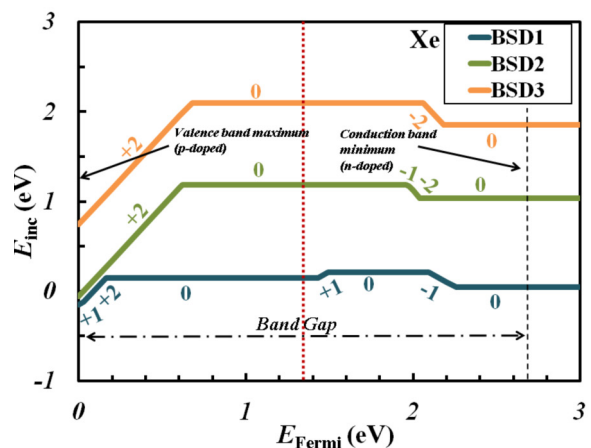
In order to have an insight into the trapping behavior of the fission gases in  $\text{CeO}_2$ , the incorporation energies of Xe and Kr atoms were calculated as a function of the Fermi energy according to Eq. (14) in various defect sites: single vacancies, divacancies, and the bound Schottky defects. There is no dependence on the stoichiometry conditions because the chemical potentials  $\mu_{\text{Ce}}^{\text{CeO}_2}$  and  $\mu_{\text{O}}^{\text{CeO}_2}$  are canceled out in the calculation of the incorporation energy.  $\Delta q = q' - q$ , the change of the charge state of the defect site before ( $q$ ) and after ( $q'$ ) the incorporation of the fission gas atom, is indicated on the corresponding curves of each defect site in Figs. 7 and 8.

### A. Incorporation energies of Xe and Kr atoms

Figure 7 shows that the highest incorporation energy for the Xe atom is found when considering incorporation in the oxygen vacancy. For the Ce vacancy, the incorporation energy strongly depends on the Fermi energy in the region above the valence-band maximum from about  $-3.7$  eV ( $p$ -doped ceria) to  $+3.1$  eV in the middle of the band gap. For the divacancy ( $\text{V}_{\text{Ce}}+\text{V}_\text{O}$ ), the incorporation energy of Xe for the Fermi energy in the middle of the band gap is 0.96 eV, which is a lower energy than the one in the mono vacancy ( $\text{V}_\text{Ce}$



(a) Small vacancy sites

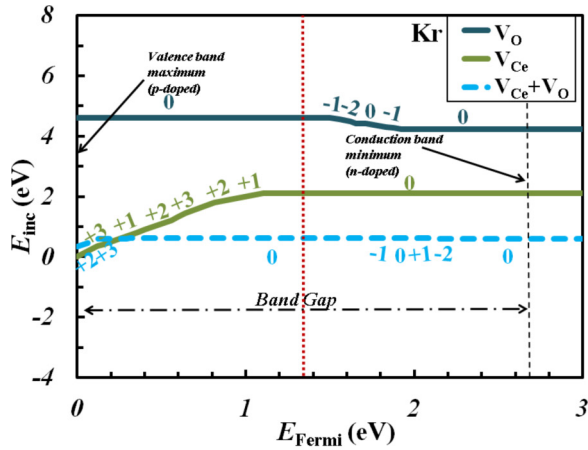


(b) Bound Schottky defect sites

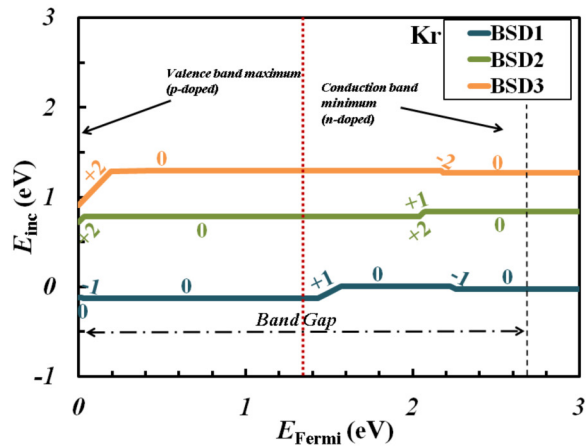
FIG. 7. Incorporation energy of Xe in defect sites of  $\text{CeO}_2$  calculated using LDA+ $U$  as a function of the Fermi energy,  $\Delta q$  is indicated on the curves of the corresponding defect sites.

or  $\text{V}_\text{O}$ ). When considering the incorporation in the bound Schottky defects, we found that the BSD1 configuration with oxygen vacancies along the (100) direction gives the lowest incorporation energy which is 0.15 eV for the Fermi energy in the middle of the band gap. Regarding geometry of the three configurations of BSD in Fig. 5, the BSD1 is more compact than the BSD2 which is more compact than the BSD3. This explains that the BSD1 is the most preferable incorporation site for Xe atoms.

For the incorporation of Kr in  $\text{CeO}_2$  (shown in Fig. 8), the preferred defect sites are found consistent with Xe. However, for Kr, the value of the Fermi energy has no effect as significant as for Xe on the incorporation energies. Table IV shows Xe and Kr incorporation energies in various defect sites for the Fermi energy in the middle of the band gap. The calculated incorporation energies of Kr are generally lower than the ones of Xe, which means that Kr is more easily incorporated in the defect sites than Xe in  $\text{CeO}_2$ . The BSD1 is still the favorable trapping site for Kr with an incorporation energy slightly lower than 0 eV for the Fermi energy in the middle of the band gap. Considering the most stable charge states of the defect sites, we can see that for both Xe and Kr,  $\Delta q$  is 0 (except for the



(a) Small vacancy sites



(b) Bound Schottky defect sites

FIG. 8. Incorporation energy of Kr in defect sites of CeO<sub>2</sub> using LDA+U as a function of the Fermi energy,  $\Delta q$  is indicated on the curves of the corresponding defect sites.

incorporation of Xe in V<sub>Ce</sub>) for the Fermi energy in the middle of band gap, which means that the most stable charge state remains unchanged after the incorporation of Xe and Kr in the defect sites. The incorporation energies for both Xe and

TABLE IV. Incorporation energies of Xe and Kr atoms in various defect sites for the Fermi energy in the middle of the band gap in CeO<sub>2</sub> using LDA+U and comparison with the corresponding values for UO<sub>2</sub> taken from the literature (GGA+U in Refs. [51,52], LDA+U in Ref. [74] where the incorporation energies were calculated from their data using Eq. (12).

Defect sites	Xe atom		Kr atom	
	CeO <sub>2</sub>	UO <sub>2</sub>	CeO <sub>2</sub>	UO <sub>2</sub>
V <sub>O</sub> (eV)	7.32	6.89 <sup>b,c</sup>	4.61	4.72 <sup>b</sup>
V <sub>Ce U</sub> (eV)	2.68	2.29 <sup>a</sup> , 3.84 <sup>b,c</sup>	2.10	2.32 <sup>b</sup>
V <sub>Ce U</sub> +V <sub>O</sub> (eV)	0.96	1.19 <sup>a</sup>	0.63	1.22 <sup>b</sup>
BSD1 (eV)	0.15	0.18 <sup>a</sup> , 1.18 <sup>b,c</sup>	-0.13	0.61 <sup>b</sup>
BSD2 (eV)	1.18	1.82 <sup>b,c</sup>	0.78	1.20 <sup>b</sup>
BSD3 (eV)	2.10	2.25 <sup>b,c</sup>	1.29	1.48 <sup>b</sup>

<sup>a</sup>Reference [74].

<sup>b</sup>Reference [51].

<sup>c</sup>Reference [52].

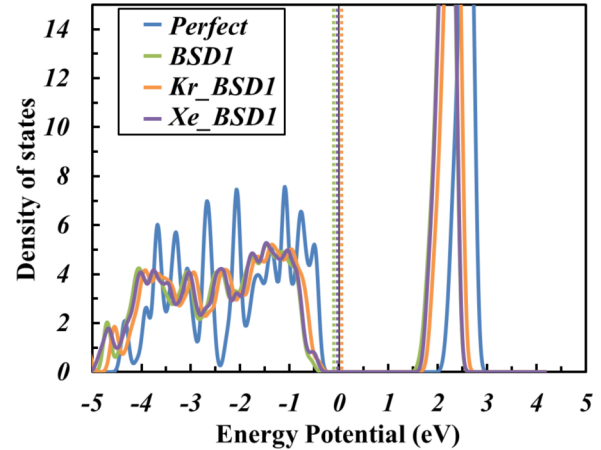


FIG. 9. Total density of states of CeO<sub>2</sub> with Kr and Xe incorporated in the BSD1 Schottky defect and comparison to the one of CeO<sub>2</sub> containing only the BSD1 and to the one of perfect CeO<sub>2</sub>. The Fermi level of perfect CeO<sub>2</sub> is fixed at 0 eV. The dashed lines present the Fermi levels for BSD1 (green), Xe in BSD1 (purple), and Kr in BSD1 (orange). The Fermi level of BSD1 (-0.1 eV), Xe in BSD1 (-0.025 eV), and Kr in BSD1 (0.025 eV) are very close to the one of perfect CeO<sub>2</sub>.

Kr in the defect sites depend on the Fermi energy when  $\Delta q$  is nonzero. The most significant variation of incorporation energies occurs for Xe incorporation into Ce vacancies and Fermi energies close to the valence-band maximum (*p*-doped case).

### B. Density of states of CeO<sub>2</sub> with Xe and Kr incorporated in the BSD1

In order to have an insight into the modification of the electronic structure of CeO<sub>2</sub> induced by fission gas atoms, we plotted in Fig. 9 the density of states of CeO<sub>2</sub> with Xe and Kr incorporated in their most favorable trapping site, that is the neutral bound Schottky defect (BSD1). The density of states for CeO<sub>2</sub> with the neutral BSD1 only and for perfect CeO<sub>2</sub> are presented as well for comparison.

We see that the densities of states of CeO<sub>2</sub> with Xe and with Kr in a BSD1 Schottky defect are very similar to each other and to the one of CeO<sub>2</sub> with the BSD1 Schottky defect only. We thus find that the incorporation of the fission gas atoms in their most favorable trapping site does not influence the electronic structure of CeO<sub>2</sub>. However, in comparison to the density of states of perfect CeO<sub>2</sub>, we find that the band gaps slightly decrease: when Xe is trapped in BSD1, the conduction band is shifted by 0.5 eV towards the valence band. And when Kr is trapped in BSD1, the conduction band is shifted by 0.4 eV towards the valence band.

### C. Comparison with UO<sub>2</sub>

Our results of the Kr and Xe incorporation in CeO<sub>2</sub> are compared with the ones obtained in UO<sub>2</sub> by Andersson *et al.* [74], Vathonne *et al.* [51], and Dorado *et al.* [52]. As already mentioned, the difference between LDA+U and GGA+U is not essential for that comparison. The same OMC scheme and the supercell-size corrections to formation and incorporation

energies were used in the studies of  $\text{UO}_2$  and  $\text{CeO}_2$ . Table IV shows the comparison of Xe and Kr incorporation energies between  $\text{CeO}_2$  and  $\text{UO}_2$ . Common features in the trapping properties of Xe and Kr between  $\text{UO}_2$  and  $\text{CeO}_2$  are found: the calculated incorporation energies of Xe and Kr in the same defect sites are in good agreement between  $\text{UO}_2$  and  $\text{CeO}_2$  for the Fermi level in the middle of the band gap; the BSD1 has the lowest incorporation energy of both Xe and Kr for  $\text{UO}_2$  and  $\text{CeO}_2$ , which means that the bound Schottky defect within this configuration is the most energetically preferable site to trap either the Xe or the Kr atoms in both compounds. Furthermore, there is a correlation between the fission gas incorporation and the vacancy size: the larger the vacancy size is, the more favorable the fission gas atoms are trapped in.

Comparing the incorporation energy graphs between  $\text{CeO}_2$  and  $\text{UO}_2$  (Ref. [51, Fig. 4.1]), we notice that the incorporation energy of Kr in the defect sites of  $\text{UO}_2$  remains almost constant ( $\Delta q = 0$ ) as a function of the Fermi energy. However, for  $\text{CeO}_2$ , we can see that the incorporation energy of Kr (but also of Xe) in  $V_{\text{Ce}}$  changes with the Fermi energy in the region between the valence-band maximum and the middle of the band gap [shown in Fig. 8(a)]. We should note that the charge states of cation vacancies are not formal for the Fermi energy in this region. The differences between  $\text{UO}_2$  and  $\text{CeO}_2$  arise since there may be  $\text{U}^{5+}$  ions created in  $\text{UO}_2$ , yet no formation of  $\text{Ce}^{5+}$  ions in  $\text{CeO}_2$  is possible. Instead of the formation of +5 valence state for Ce, the incorporation of the Kr atom in  $V_{\text{Ce}}$  results in the charge loss on the  $4p$  orbitals of the Kr atom and the  $2p$  orbitals of the eight neighboring O atoms in  $\text{CeO}_2$ . Bader charge analysis indeed shows that after the incorporation of one Kr atom in the cation vacancy under nonformal charge states, the Kr atom loses some charge in  $\text{CeO}_2$  but not in  $\text{UO}_2$ . For instance, for nonformal charge states of  $V_{\text{Ce}}$ , the Kr atom loses charge up to  $0.8 |e|$  from Bader charge analysis. This charge loss behavior has also been found in our study of the incorporation of Xe into the Ce vacancy, which agrees well with Xiao *et al.*'s study showing the same Bader charge loss of  $1.4 |e|$  for a Xe atom in a neutral  $V_{\text{Ce}}$  [38].

This charge loss behavior constitutes the main difference between  $\text{UO}_2$  and  $\text{CeO}_2$  for the incorporation of Xe and Kr in defect sites. However, it does not appear for a Fermi energy close to the middle of the band gap where the most stable trap sites are under their formal charge state. In addition, considering the significant common features found in this section between these two compounds, we can conclude that the incorporation properties of the fission gases Xe and Kr are similar in  $\text{CeO}_2$  and in  $\text{UO}_2$ .

## VI. CONCLUSIONS

In this study, we investigated the formation of various charged defects and the incorporation of the fission gas atoms Xe and Kr in  $\text{CeO}_2$ . The electron potential (Fermi energy) is an important factor that influences the formation and incorporation energies of small and large charged defects. By calculating the formation energy of defects under various charge states in  $\text{CeO}_2$ , great similarity was found between  $\text{CeO}_2$  and  $\text{UO}_2$ . For the incorporation of fission gas atoms,  $\text{CeO}_2$  and  $\text{UO}_2$  have similar trapping properties of Xe and Kr atoms. The bound Schottky defect BSD1 is the most energetically preferable site to host fission gas atoms in both compounds. So, we can conclude that  $\text{CeO}_2$  could largely simulate  $\text{UO}_2$  under stoichiometric and nonstoichiometric conditions. That is true for nearly all positions of the Fermi energy within the band gap besides the heavily  $p$ -doped case (Fermi level close to the valence-band maximum). Let us note that a certain difference between  $\text{UO}_2$  and  $\text{CeO}_2$  exists for the incorporation of Xe and Kr atoms in the cation sites under nonformal charge states: Xe and Kr atoms lose charge in  $\text{CeO}_2$  but not in  $\text{UO}_2$ , leading to differences in the incorporation energies. The reason is the absence of the +5 valence state for Ce in contrast to its existence for U. However, this difference between  $\text{CeO}_2$  and  $\text{UO}_2$  is not found for the defect sites under their formal charge state, which is their favorable configuration for the Fermi level near the middle of the band gap. Therefore it does not influence the good agreement of the incorporation properties of Xe and Kr between  $\text{CeO}_2$  and  $\text{UO}_2$ .

Based on those common features on point defects and fission gas atoms that we have obtained by DFT+ $U$  calculations for  $\text{CeO}_2$  and  $\text{UO}_2$ , we could conclude that our study contributes to justify the following assumption:  $\text{CeO}_2$  might be considered as a surrogate of  $\text{UO}_2$  to study experimentally the radiation damage. However, our study is only one of the first step to ascertain the similarities of  $\text{UO}_2$  and  $\text{CeO}_2$  in terms of radiation damage. More investigations could be conducted to compare the atomic transport properties of defects and fission gases, grain boundary behavior and fission gas release in  $\text{UO}_2$  and  $\text{CeO}_2$  using the relevant modeling techniques.

## ACKNOWLEDGMENTS

This work was partly performed using HPC resources from "Grand Équipement National de Calcul Intensif" (GENCI) grant x2015096008. The authors thank M. Bertolus, G. Jomard, and J. Wiktor for useful discussions.

- 
- [1] A. F. Kohan, G. Ceder, D. Morgan, and C. G. Van de Walle, *Phys. Rev. B* **61**, 15019 (2000).
  - [2] M. Yashima, *J. Phys. Chem. C* **113**, 12658 (2009).
  - [3] T. Désaunay, B. Medina-Lott, A. Ringuedé, M. Cassir, C. Adamo, and F. Labat, *ECS Transactions* **35**, 1015 (2011).
  - [4] *Catalysis by Ceria and Related Materials*, 2nd ed., edited by A. Trovarelli and P. Fornasiero, Catalytic Science Series Vol. 12 (Imperial College Press, London, 2013).
  - [5] J. S. Sim, J. Shi, and S. Ramanathan, *J. Mater. Chem. A* **2**, 19019 (2014).
  - [6] T. Montini, M. Melchionna, M. Monai, and P. Fornasiero, *Chem. Rev.* **116**, 5987 (2016).
  - [7] D. R. Mullins, S. H. Overbury, and D. R. Huntley, *Surf. Sci.* **409**, 307 (1998).
  - [8] E. Wuilloud, B. Delley, W. D. Schneider, and Y. Baer, *Phys. Rev. Lett.* **53**, 202 (1984).

- [9] A. Iwase, H. Ohno, N. Ishikawa, Y. Baba, N. Hirao, T. Sonoda, and M. Kinoshita, *Nucl. Instrum. Methods Phys. Res., Sect. B* **267**, 969 (2009).
- [10] H. Ohno, A. Iwase, D. Matsumura, Y. Nishihata, J. Mizuki, N. Ishikawa, Y. Baba, N. Hirao, T. Sonoda, and M. Kinoshita, *Nucl. Instrum. Methods Phys. Res., Sect. B* **266**, 3013 (2008).
- [11] K. Shimizu, S. Kosugi, Y. Tahara, K. Yasunaga, Y. Kaneta, N. Ishikawa, F. Hori, T. Matsui, and A. Iwase, *Nucl. Instrum. Methods Phys. Res., Sect. B* **286**, 291 (2012).
- [12] V. Fernandes, P. Schio, A. J. A. d. Oliveira, W. A. Ortiz, P. Fichtner, L. Amaral, I. L. Graff, J. Valada, N. Mattoso, W. H. Schreiner, and D. H. Mosca, *J. Phys.: Condens. Matter* **22**, 216004 (2010).
- [13] M. Li, S. Ge, W. Qiao, L. Zhang, Y. Zuo, and S. Yan, *Appl. Phys. Lett.* **94**, 152511 (2009).
- [14] N. V. Skorodumova, R. Ahuja, S. I. Simak, I. A. Abrikosov, B. Johansson, and B. I. Lundqvist, *Phys. Rev. B* **64**, 115108 (2001).
- [15] P. J. Hay, R. L. Martin, J. Uddin, and G. E. Scuseria, *J. Chem. Phys.* **125**, 034712 (2006).
- [16] H. X. Song, L. Liu, H. Y. Geng, and Q. Wu, *Phys. Rev. B* **87**, 184103 (2013).
- [17] J. J. Plata, A. M. Márquez, and J. F. Sanz, *J. Chem. Phys.* **136**, 041101 (2012).
- [18] C. Loschen, J. Carrasco, K. M. Neyman, and F. Illas, *Phys. Rev. B* **75**, 035115 (2007).
- [19] J. L. F. Da Silva, M. V. Ganduglia-Pirovano, J. Sauer, V. Bayer, and G. Kresse, *Phys. Rev. B* **75**, 045121 (2007).
- [20] R. Gillen, S. J. Clark, and J. Robertson, *Phys. Rev. B* **87**, 125116 (2013).
- [21] D. A. Andersson, S. I. Simak, B. Johansson, I. A. Abrikosov, and N. V. Skorodumova, *Phys. Rev. B* **75**, 035109 (2007).
- [22] N. V. Skorodumova, S. I. Simak, B. I. Lundqvist, I. A. Abrikosov, and B. Johansson, *Phys. Rev. Lett.* **89**, 166601 (2002).
- [23] S. Fabris, S. de Gironcoli, S. Baroni, G. Vicario, and G. Balducci, *Phys. Rev. B* **71**, 041102 (2005).
- [24] T. Zacherle, A. Schrieffer, R. A. De Souza, and M. Martin, *Phys. Rev. B* **87**, 134104 (2013).
- [25] M. Iwasawa, T. Ohnuma, Y. Chen, Y. Kaneta, H.-Y. Geng, A. Iwase, and M. Kinoshita, *J. Nucl. Mater.* **393**, 321 (2009).
- [26] Y. Jiang, J. B. Adams, M. v. Schilfsgaarde, R. Sharma, and P. A. Crozier, *Appl. Phys. Lett.* **87**, 141917 (2005).
- [27] H.-Y. Li, H.-F. Wang, X.-Q. Gong, Y.-L. Guo, Y. Guo, G. Lu, and P. Hu, *Phys. Rev. B* **79**, 193401 (2009).
- [28] C. W. M. Castleton, J. Kullgren, and K. Hermansson, *J. Chem. Phys.* **127**, 244704 (2007).
- [29] H. Y. Xiao and W. J. Weber, *J. Phys. Chem. B* **115**, 6524 (2011).
- [30] M. Nolan, S. C. Parker, and G. W. Watson, *Surf. Sci.* **595**, 223 (2005).
- [31] M. Nolan, J. E. Fearon, and G. W. Watson, *Solid State Ionics* **177**, 3069 (2006).
- [32] P. R. L. Keating, D. O. Scanlon, B. J. Morgan, N. M. Galea, and G. W. Watson, *J. Phys. Chem. C* **116**, 2443 (2012).
- [33] P. R. L. Keating, D. O. Scanlon, and G. W. Watson, *J. Mater. Chem. C* **1**, 1093 (2013).
- [34] J.-F. Jerratsch, X. Shao, N. Nilius, H.-J. Freund, C. Popa, M. V. Ganduglia-Pirovano, A. M. Burow, and J. Sauer, *Phys. Rev. Lett.* **106**, 246801 (2011).
- [35] G. E. Murgida, V. Ferrari, M. V. Ganduglia-Pirovano, and A. M. Llois, *Phys. Rev. B* **90**, 115120 (2014).
- [36] M. V. Ganduglia-Pirovano, J. L. F. Da Silva, and J. Sauer, *Phys. Rev. Lett.* **102**, 026101 (2009).
- [37] Y. Miao, W.-Y. Chen, A. Oaks, K. Mo, and J. F. Stubbins, *J. Nucl. Mater.* **449**, 242 (2014).
- [38] H. Y. Xiao, Y. Zhang, and W. J. Weber, *J. Nucl. Mater.* **414**, 464 (2011).
- [39] B. Dorado, B. Amadon, M. Freyss, and M. Bertolus, *Phys. Rev. B* **79**, 235125 (2009).
- [40] B. Dorado, G. Jomard, M. Freyss, and M. Bertolus, *Phys. Rev. B* **82**, 035114 (2010).
- [41] G. Jomard, B. Amadon, F. Bottin, and M. Torrent, *Phys. Rev. B* **78**, 075125 (2008).
- [42] B. Amadon, F. Jollet, and M. Torrent, *Phys. Rev. B* **77**, 155104 (2008).
- [43] P. Larson, W. R. L. Lambrecht, A. Chantis, and M. van Schilfsgaarde, *Phys. Rev. B* **75**, 045114 (2007).
- [44] G. Kresse and J. Furthmüller, *Phys. Rev. B* **54**, 11169 (1996).
- [45] G. Kresse and D. Joubert, *Phys. Rev. B* **59**, 1758 (1999).
- [46] P. E. Blöchl, *Phys. Rev. B* **50**, 17953 (1994).
- [47] J. P. Perdew, K. Burke, and M. Ernzerhof, *Phys. Rev. Lett.* **77**, 3865 (1996).
- [48] D. M. Ceperley and B. J. Alder, *Phys. Rev. Lett.* **45**, 566 (1980).
- [49] S. L. Dudarev, G. A. Botton, S. Y. Savrasov, C. J. Humphreys, and A. P. Sutton, *Phys. Rev. B* **57**, 1505 (1998).
- [50] E. Vathonne, J. Wiktor, M. Freyss, G. Jomard, and M. Bertolus, *J. Phys.: Condens. Matter* **26**, 325501 (2014).
- [51] E. Vathonne, Ph.D. thesis, Aix Marseille University, 2014.
- [52] B. Dorado, Ph.D. thesis, Aix Marseille University, 2010.
- [53] L. Gerward, J. Staun Olsen, L. Petit, G. Vaitheeswaran, V. Kanchana, and A. Svane, *J. Alloys Compd.* **400**, 56 (2005).
- [54] A. Nakajima, A. Yoshihara, and M. Ishigame, *Phys. Rev. B* **50**, 13297 (1994).
- [55] R. J. M. Konings, O. Beneš, A. Kovács, D. Manara, D. Sedmidubský, L. Gorokhov, V. S. Iorish, V. Yungman, E. Shenayavskaya, and E. Osina, *J. Phys. Chem. Ref. Data* **43**, 013101 (2014).
- [56] E. Voloshina and B. Paulus, *J. Chem. Phys.* **124**, 234711 (2006).
- [57] S. E. Taylor and F. Bruneval, *Phys. Rev. B* **84**, 075155 (2011).
- [58] M. Leslie and N. J. Gillan, *J. Phys. C: Solid State* **18**, 973 (1985).
- [59] S. Lany and A. Zunger, *Model. Simul. Mater. Sc.* **17**, 084002 (2009).
- [60] N. I. Santha, M. T. Sebastian, P. Mohanan, N. M. Alford, K. Sarma, R. C. Pullar, S. Kamba, A. Pashkin, P. Samukhina, and J. Petzelt, *J. Am. Ceram. Soc.* **87**, 1233 (2004).
- [61] C. B. Carter and M. G. Norton, in *Ceramic Materials* (Springer, New York, 2013), pp. 53–72.
- [62] S. Na-Phattalung, M. F. Smith, K. Kim, M.-H. Du, S.-H. Wei, S. B. Zhang, and S. Limpijumnong, *Phys. Rev. B* **73**, 125205 (2006).
- [63] M. Hong, S. R. Phillpot, C.-W. Lee, P. Nerikar, B. P. Uberuaga, C. R. Stanek, and S. B. Sinnott, *Phys. Rev. B* **85**, 144110 (2012).
- [64] S. Kurth, J. P. Perdew, and P. Blaha, *Int. J. Quantum Chem.* **75**, 889 (1999).
- [65] Y.-L. Lee, J. Kleis, J. Rossmeisl, and D. Morgan, *Phys. Rev. B* **80**, 224101 (2009).
- [66] L. Wang, T. Maxisch, and G. Ceder, *Phys. Rev. B* **73**, 195107 (2006).
- [67] S. Grindy, B. Meredig, S. Kirklin, J. E. Saal, and C. Wolverton, *Phys. Rev. B* **87**, 075150 (2013).

- [68] S. Middleburgh, G. Lumpkin, and R. Grimes, *Solid State Ionics* **253**, 119 (2013).
- [69] M. Zinkevich, D. Djurovic, and F. Aldinger, *Solid State Ionics* **177**, 989 (2006).
- [70] J. Reader and G. L. Epstein, *J. Opt. Soc. Am.* **65**, 638 (1975).
- [71] N. C. Pyper and I. P. Grant, *J. Chem. Soc., Faraday Trans. 2* **74**, 1885 (1978).
- [72] W. M. Haynes, *CRC Handbook of Chemistry and Physics*, 96th ed. (2015), Sec. 10: Ionization Energies of Atoms and Atomic Ions.
- [73] Y. A. Mastrikov, R. Merkle, E. Heifets, E. A. Kotomin, and J. Maier, *J. Phys. Chem. C* **114**, 3017 (2010).
- [74] D. A. Andersson, B. P. Uberuaga, P. V. Nerikar, C. Unal, and C. R. Stanek, *Phys. Rev. B* **84**, 054105 (2011).